Near-field optical spectroscopy of GaAs/$Al_yGa_{1-y}As$ quantum dot pairs grown by high-temperature droplet epitaxy

Robert Pomraenke,[1,2,*] Christoph Lienau,[1,2] Yuriy I. Mazur,[3] Zhiming M. Wang,[3] Baolai Liang,[3] Georgiy G. Tarasov,[3,†] and Gregory J. Salamo[3]

[1]*Institut für Physik, Carl von Ossietzky Universität Oldenburg, D-26111 Oldenburg, Germany*

[2]*Max-Born-Institut für Nichtlineare Optik und Kurzzeitspektroskopie, D-12489 Berlin, Germany*

[3]*Department of Physics, University of Arkansas, Fayetteville, Arkansas 72701, USA*

(Received 28 January 2007; revised manuscript received 18 October 2007; published 14 February 2008)

We report a near-field photoluminescence study of pairs of GaAs quantum dots grown by droplet epitaxy, a growth mode for fabricating quantum dot arrays with controlled geometries. Our study reveals the optical properties of the *individual* quantum dots within each pair and, by means of a statistical analysis, the correlation between *geometrical* and *optical* properties of such arrays. Due to their high optical quality and unique geometry, ordered droplet epitaxy quantum dot arrays may become interesting candidates for coherent exciton and/or spin manipulation.

DOI: 10.1103/PhysRevB.77.075314 PACS number(s): 42.70.Qs, 07.79.Fc, 42.25.−p, 73.20.Mf

I. INTRODUCTION

The fabrication of semiconductor quantum dot (QD) arrays with controlled geometries is a challenging and fascinating current activity in solid-state research. During the past few years, the coherent manipulation of charge and spin excitations of QDs has seen encouraging progress toward applications to quantum logic. For example, Rabi oscillations,[1,2] a conditional two-qubit gate based on exciton-biexciton transitions,[3] strong coupling to photons,[4–6] and dipolar coupling in a pair of quantum dots[7] have been demonstrated. In addition, manipulation of optically induced spins in quantum dots is currently pursued in various laboratories[8,9] and, most recently, single spin Rabi oscillations have been demonstrated using radio-frequency excitation.[10] These first steps toward quantum information processing are relevant because QD systems offer, at least conceptually, the potential of implementing scalable arrays of quantum bits. The fabrication of QD arrays, however, is challenging due to the inherent size and composition fluctuations in QD ensembles and the difficulty of achieving controlled spatial ordering.

Different strategies have been explored for generating vertical or lateral ordering of QDs, such as using vertical strain,[6,11–13] templates,[14] or lithography.[15] Most recently, droplet epitaxy using lattice-matched semiconductors has emerged as a novel, promising technique for fabricating geometrically controlled QD pairs, rings or even more complex QD arrays, all of high optical quality.[16–20] While some recent studies have reported on single QD photoluminescence using this growth approach,[21] very little is known about the optical properties of more complex nanostructures. In particular, correlation studies between the complex structural and optical properties are still lacking.

In this paper, we present a near-field spectroscopic study of pairs of QDs grown by droplet epitaxy. By spectrally resolving and spatially imaging excitonic and biexcitonic emission lines, we are able to resolve the optical properties of the individual dots within such a pair. A near-field autocorrelation analysis shows that the unique geometrical property of the QD pair is preserved during overgrowth and is directly reflected in the near-field optical spectra. This result points to the potential use of droplet epitaxy of ordered QD arrays for studies in quantum logic.

II. EXPERIMENT

For this investigation, GaAs quantum dot pairs (QDPs) were grown by molecular beam epitaxy on a semi-insulating GaAs (100) substrate. The samples were fabricated by depositing a 500 nm GaAs buffer layer and a 50 nm thick $Al_{0.3}Ga_{0.7}As$ layer, followed by deposition of Ga and the formation of Ga droplets at a substrate temperature of 550 °C with the arsenic source being fully closed. The total amount of Ga deposited was equal to an amount that would normally result in 10.0 ML of GaAs growth. Subsequently, the Ga droplets were "arsenized" into GaAs QDP oriented along the [0−11] direction by fine control of the arsenic flux and the corresponding annealing period.[17,18] The current understanding is that the QDP forms due to the anisotropic surface diffusion of Ga adatoms during crystallization.[16–21] After growth, the surface morphology of the QDP samples was characterized using an atomic force microscope (AFM) under ambient conditions. Meanwhile, for optical characterization, the QDPs were buried by deposition of 50 nm of an $Al_{0.3}Ga_{0.7}As$ barrier layer and a 20 nm GaAs cap layer.

Photoluminescence (PL) spectra from an ensemble of QDP were recorded in a variable temperature 8–300 K closed-cycle cryostat using a Nd:YAG (where YAG denotes yttrium aluminum garnet) laser at 532 nm as the excitation source. For these measurements, the laser light was focused to a diameter ~30 μm and the excitation power was varied between 0.3 μW and 10 mW. The PL signal from the sample was dispersed using a monochromator and detected by a nitrogen-cooled InGaAs photodiode array. For high spatial resolution imaging of *individual* QDP luminescence, however, we used a low-temperature near-field scanning optical microscope operating at a temperature of 15 K inside a high vacuum chamber.[22] In this case, optical excitation was provided by a helium-neon laser at 632 nm at power levels of

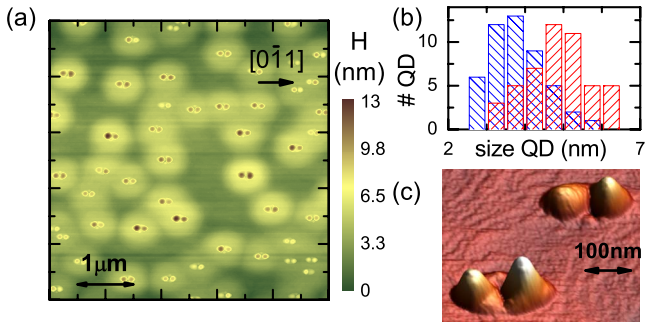

FIG. 1. (Color online) (a) AFM image of the quantum dot pair sample before overgrowth. The individual pairs have an interdot distance of about 130 nm and are aligned along the [0−11] direction. The dots with a height of 10 nm reside on a shallow base with a diameter of 300 nm. (b) Size distribution for all small QDs (blue) and all big QDs (red) in each QDP. (c) Three-dimensional plot of a zoom into the AFM image. Shown are images of two adjacent QD pairs. The height scale is 15 nm.

0.5 nW–0.5 μW, which was coupled into a chemically etched, uncoated single mode fiber.[23] The local PL signal was collected through the same fiber tip, dispersed using a spectrometer (with f=50 cm and resolution ~100 μeV), and recorded with a nitrogen-cooled charge-coupled device camera. For spatial PL imaging, the fiber probe was raster scanned across the sample surface in a 4.8×4.8 μm^2 area with a pixel of 80 nm. At every pixel, a full PL spectrum was recorded within an integration time of 0.5 s. A constant tip-to-sample distance of 15 nm was maintained during scanning by means of a shear-force distance control.[24] This near-field optical technique simultaneously demonstrated excellent PL detection efficiency and a spatial resolution down to 160 nm.[25] For the studies reported here, the spatial resolution was held at 300 nm.

III. RESULTS

A typical AFM image of the QDP sample is shown in Fig. 1(a). The image reveals the almost perfect alignment of the quantum dot pairs along the [0−11] direction and a rather low QDP density of about 2.3 QDPs per μm^2. A zoom into these images [Fig. 1(c)] gives an average interdot distance within each pair of 130 nm. The height of individual QDs is about 5 nm, and each pair resides on a flat and rather extended 4 nm high GaAs base with a diameter of about 500 nm. This picture is confirmed by additional x-ray diffuse scattering measurements of the uncapped sample, showing completely strain-free QDPs aligned along the [0−11] direction with a 135 nm inner distance.[26] For all QDs, from Fig. 1(a) the height was estimated, and the height distributions for the small and large QDs within each QDP are shown in Fig. 1(b). Figure 1(b) indicates an average height of 3.5 nm and of 5.0 nm for the small and large QDs, respectively. Clearly, the height of the two QDs within each pair is not the same, but differs by about 30%.

Low-temperature (T=10 K) PL spectra of the QDP ensembles at a moderate excitation intensity of about 3 W/cm^2 [Fig. 2(a)] reveal two distinct PL bands assigned to QDP

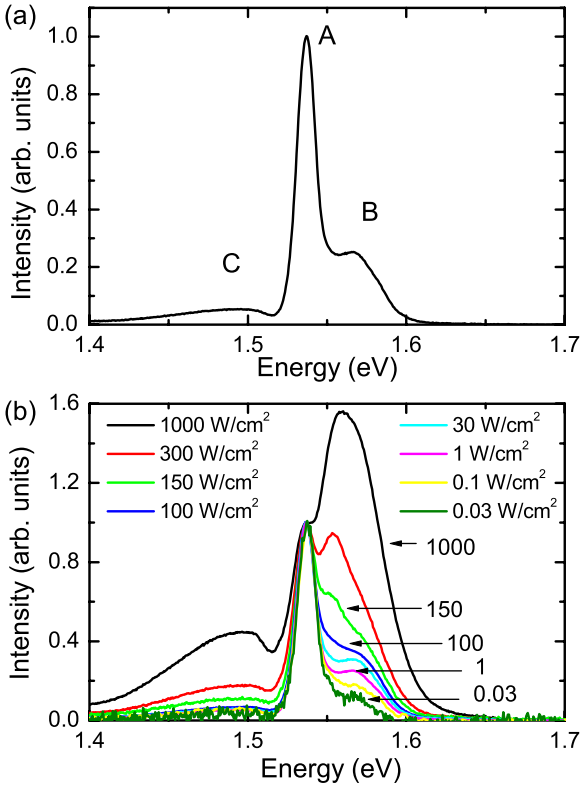

FIG. 2. (Color online) (a) Typical macroscopic PL spectrum of an ensemble of QDPs at low excitation intensity (1 W/cm^2) recorded with a spatial resolution of 30 μm. At this intensity, the emission bands A and B reflect the inhomogeneously broadened emission ground state exciton emission spectra of the individual quantum dots within each pair. (b) Macroscopic PL spectra recorded with a spot size of 30 μm for different excitation intensities between 0.03 and 1000 W/cm^2. The spectra are normalized to the maximum emission of peak A. With increasing excitation power, the emission from peak A saturates and peak B dominates the total PL signal.

emission: (i) a low-energy band A with a maximum at E_A =1.536 eV and a full width at half maximum (FWHM) Γ_A ~10 meV; and (ii) a high-energy band at E_B=1.567 eV and Γ_B~29 meV. Both PL resonances are spectrally quite narrow and even for the high-energy band, with a FWHM three times larger than that of band A, the width is considerably smaller than for typical self-assembled QDs grown in the Stranski-Krastanov mode. The far-field spectra of such QDs are governed by inhomogeneous broadening, and the comparatively narrow width of our spectra, therefore, reflects the good size homogeneity of the QD ensemble grown by high-temperature droplet epitaxy.

We tentatively assign these two resonances to the emission from the two individual QDs within each QDP [supported by the size distribution shown in Fig. 1(b)]. Power dependent macroscopic PL spectra are shown in Fig. 2(b). Up to an excitation intensity of ~100 W/cm^2, the PL intensity of band A increases linearly and then begins to saturate. At the lowest excitation intensity, the maximum emission intensity of band B is about a factor of 8 less than that of band A. When normalized to the intensity of the PL maximum of band A, the relative weight of band B increases

monotonously with increasing excitation intensity and this band begins to dominate the emission at intensities above 300 W/cm^2. This intensity dependence is most likely explained by the saturation of the ground state exciton emission due to state filling of the—geometrically slightly larger—low-energy QDs and the—geometrically slightly smaller—high-energy QDs. The nonlinear increase in emission intensity of band B then arises from an increasing excited state emission from both QDs at high excitation intensities. This interpretation is supported by the near-field spectroscopic experiments discussed below.

Apart from these QD-related emission bands, the spectra at high intensities also show a broad background emission around 1.5 eV. In high-quality GaAs materials, emission in this spectral region is generally due to recombination processes involving shallow acceptors, i.e., free electron–bound acceptors and donor-to-acceptor pair transitions.[27] Here, it is likely that such acceptors are mostly located within the 4 nm high GaAs base surrounding the QDs. We note that, apart from these acceptor transitions, we observe no clear signature of the GaAs base in photoluminescence. This indicates that transfer of carriers within the GaAs base and subsequent trapping into the quantum dots[22] are fast compared to the QD PL decay time and highly efficient.

Based on the macroscopic far-field photoluminescence spectra alone, it is difficult to unambiguously verify this assignment because various alternative interpretations are possible. For example, multiexcitonic transitions[28] or even excited states within a pair of electronically coupled QDs are possible. Also, interdot exciton relaxation processes can largely affect those spectra. Therefore, it is particularly interesting to analyze the optical properties of the QDPs by probing them individually. This is challenging because of the small geometric separation of only about 100 nm between the individual QDs of each QDP. We, therefore, decided to use low-temperature near-field scanning optical microscopy in order to obtain spatially highly resolved spectroscopic characterization. In order to have sufficient flexibility in varying the excitation conditions, we used an uncoated, chemically etched near fiber probe[29] using the illumination-collection geometry. In this geometry, the sample was locally excited by transmitting the He-Ne laser light through the near-field probe and collecting the emitted PL via the same fiber. As already mentioned, this geometry provides spatial and spectral resolutions of less than 200 nm and 100 μeV, respectively.[25] A spectrally integrated near-field photoluminescence image of the QDP sample within a scan range of 4.8×4.8 μm^2 is shown in Fig. 3(a). The image is taken at a temperature of 15 K by raster scanning the near-field probe at constant probe-to-sample distance across the sample with a step size of 80 nm. The sample is excited at the photon energy of 1.959 eV with an intensity of 75 W/cm^2. Every pixel of the imaged PL spectrum $I_{PL}(x,y,\lambda)$ is recorded in the detection range between 1.532 and 1.602 eV. The integrated intensity of this spectrum $\bar{I}(x,y)=\Sigma_{i\lambda}I(x,y,\lambda_{i\lambda})$ is then plotted as a function of the position of the near-field probe. In this image, the emission from the individual QDPs is clearly resolved. The spatial density of the luminescent QDPs is the same as that of the QDPs in the AFM image

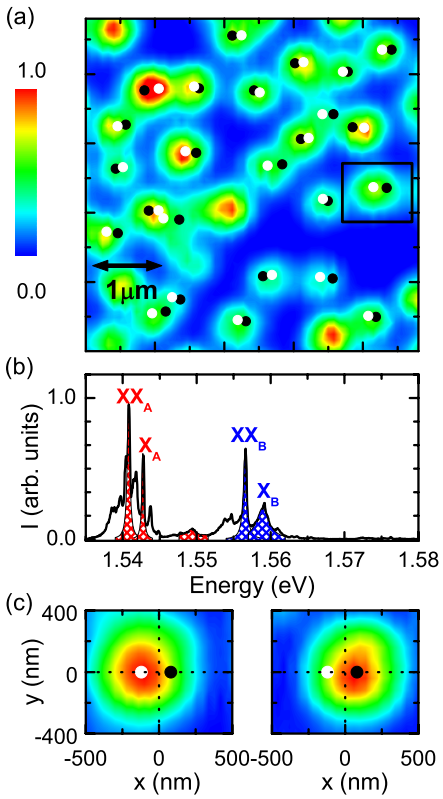

FIG. 3. (Color online) (a) Two-dimensional near-field image of total PL intensity of the QDP sample. The QDP sample is illuminated by a He-Ne laser at an intensity of about 75 W/cm^2, and a full near-field PL spectrum is recorded in the energy range between 1.532 and 1.602 eV at every pixel of the image. The integrated intensity of this spectrum is then plotted as a function of the position of the near-field probe, as it is scanned with a step size of 80 nm within a 4.8×4.8 μm^2 area. The spatial position of the individual QDs within each QD pair, as extracted from the near-field spectra (b) and (c), is indicated by a white (black) dot for the low-energy dot A and high-energy dot B, respectively. (b) Representative near-field spectrum of a single QD pair in the region indicated by the black square in (a). (c) Spatial images of the PL intensity at detection energies of 1.543 eV (QD-A) and 1.559 eV (QD-B). The image is recorded by scanning the near-field probe with a step size of 60 nm. For this particular QD pair, the images show the alignment along the $[0-11]$ (x) direction and indicate an interdot distance of 200 ± 20 nm.

[Fig. 2(a)], demonstrating that essentially all of the QDPs are optically active. We also note that the integrated PL intensity shows very little variation from one QD to the next, which is another signature of the high optical quality of the QDs in every QDP.

Due to the finite spatial resolution of our measurement technique, it is not yet possible to resolve signatures of the individual QDs of each QDP in these spectrally integrated images. However, this information can be obtained by investigating the local photoluminescence spectra. We focus on the single QD pair marked by a black square in Fig. 3(a). A representative local near-field PL spectrum in this region is shown in Fig. 3(b). We observe a series of spectrally sharp emission lines in the regions around 1.54 and 1.56 eV, reflecting the emission from different exciton states localized

within this QDP. Despite the comparatively high excitation intensities, the spectral width of most resonances is quite narrow, and falls in the range of 0.2–0.5 meV, slightly above our monochromator resolution. These comparatively sharp resonances are different from the rather broad emission lines with a width of several meV recently observed from single QDs grown by low-temperature droplet epitaxy[21] and highlight again the high optical quality of the QDP sample. Using the more precise information on the spatial intensity distribution of the individual emission lines from our near-field experiments, it becomes possible to deduce the spatial origin of the different emission lines. Such an analysis is shown in Fig. 3(c) for the two emission lines at 1.543 and 1.559 eV in Fig. 3(b). It is evident that the spatial center of the two emission peaks is shifted by 200 ± 20 nm along the x direction, i.e., along the $[0-11]$ direction. We find, however, no measurable shift along the y direction, i.e., along the [011] direction. This demonstrates clearly that the near-field spectra allow us to separately probe the optical spectra of the two individual quantum dots (A and B) within each pair. Based on this spatial selectivity, we can assign most of the lines in the low-energy region around 1.54 eV to originate from QD-A, whereas the high-energy lines around 1.56 eV are mostly related to emission from quantum-confined exciton states of QD-B. As we will demonstrate below, it is likely that the sharp lines at 1.5428 and 1.5408 eV arise from exciton (X) and biexciton (XX) emission of QD-A, whereas those at 1.5591 and 1.5566 eV can be assigned to the X and XX emission from QD-B.

Before we further support this assignment, it is interesting to ask whether this observation of spatially distinct emission peaks from the individual dots of the QDP is representative for this class of quantum dots. To address this question, we perform a statistical analysis of the local PL spectra of more than 30 different QDPs from several spatial scans including the one shown in Fig. 3(a). For each of about $N=60$ sharp and intense emission lines, $i=1,\ldots,N$, we extract the spatial position $\vec{r}_i$ of the emission center from plots similar to those in Fig. 3(c). Using these center positions, spatial autocorrelation images $g(\vec{r})=\frac{1}{N(N-1)}\Sigma_i\Sigma_{j\neq i}\delta(\vec{r}_i-\vec{r}_j-\vec{r})$ are calculated by using a Gaussian function with a FWHM of 20 nm for $\delta(\vec{r})$. Similar autocorrelation images are also recorded from the AFM images shown in Fig. 1(a). Here, $\vec{r}_i$ corresponds to the center position of one of the two QDs within each pair. The results of the autocorrelation images from AFM and near-field scanning optical spectroscopy are compared in Fig. 4. The AFM images [Fig. 4(a)] show two clear correlation peaks at positions $\vec{r}_c=(\pm 130\ \text{nm}, 0\ \text{nm})$, reflecting the average interdot separation of 130 ± 10 nm inside each quantum dot pair and the QDP alignment along the $[0-11]$ axis. The clear clustering of the correlation peaks from the individual dots (white dots) and the narrow width of the ensemble-averaged correlation peak reflect small fluctuations of the interdot spacing and, thus, the excellent size homogeneity of the fabricated QD pairs. In the optical measurements [Fig. 4(b)], individual correlation peaks (white dots) are certainly more spatially disordered than in the AFM data. Yet, the ensemble-averaged correlation function $g(\vec{r})$ still shows two clear correlation peaks at essentially the same spatial positions $\vec{r}_c=(\pm 150\ \text{nm} \pm 25\ \text{nm}, 0\ \text{nm})$ as in the AFM measurements. This striking result proves directly that the geometric ordering of the QDPs is maintained during overgrowth and governs the optical properties of the QDPs. At present, we attribute the larger disorder of the optical data mainly to the significantly reduced spatial resolution of the optical measurements compared to the AFM resolution of only 20 nm. We, thus, cannot yet rule out that the overgrowth procedure results in additional size fluctuations of the QDPs. More detailed optical studies with improved spatial resolution will certainly give more information on this question.

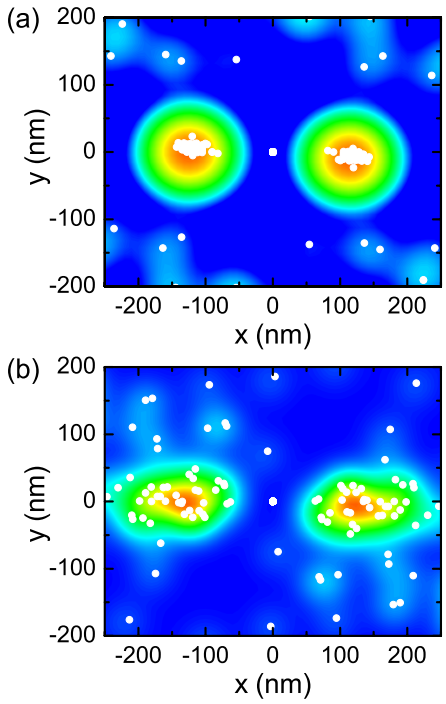

FIG. 4. (Color online) Spatial autocorrelation images $g(\vec{r})=\frac{1}{N(N-1)}\Sigma_i\Sigma_{j\neq i}\delta(\vec{r}_i-\vec{r}_i-\vec{r})$ calculated from (a) atomic force microscopy and (b) near-field scanning optical microscopy. In both cases, the center position $\vec{r}_i(i=1,\ldots,N)$ of a series of more than 60 emission lines from an ensemble of about 30 quantum dot pairs is analyzed and the autocorrelation function is then calculated by using a Gaussian function with a full width at half maximum of 20 nm for $\delta(\vec{r})$. These measurements clearly evidence the correlation between geometric and optical properties of the QD pairs. They highlight the QDP alignment along $[0-11]$ and indicate an interdot distance of (a) 130 ± 10 nm and (b) 150 ± 25 nm.

IV. DISCUSSION

Based on this information, we can now attempt to analyze the energetic structure of the QDPs. The macroscopic PL spectra (Fig. 2) indicated already a clustering of the emission lines into the inhomogeneously broadened bands A and B. This clustering is clearly seen when comparing near-field PL spectra from different QD pairs [Figs. 5(a) and 5(b)].

Such spectra consistently show a series of few emission lines centered around 1.54 eV from the geometrically somewhat larger quantum dot A and a second series of emission

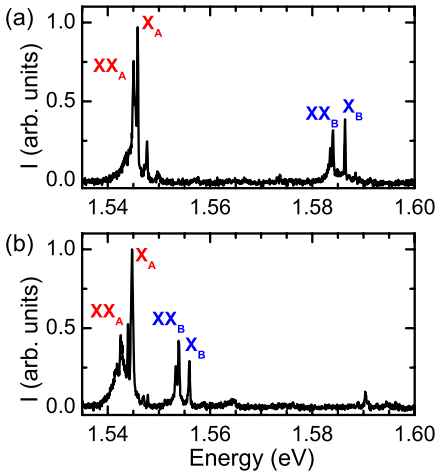

FIG. 5. (Color online) [(a) and (b)] Representative near-field PL spectra of two different quantum dot pairs recorded at an excitation intensity of 25 W/cm^2 and assignment of the PL lines to the X and XX emissions of the individual low (A) and high (B) energy dots within each QD pair.

lines fluctuating more strongly in energy range between 1.55 and 1.6 eV. These high-energy lines are assigned to the geometrically slightly smaller quantum dot B. This unambiguously shows that bands A and B in the macroscopic PL spectra are due to the geometrically larger QD-A and to the geometrically smaller QD-B within each quantum dot pair, respectively. A narrow size inhomogeneity of the larger QD-A explains the narrow width of the A band. Finally, studying the intensity dependence of near-field PL spectra allows one to explain the origin of most of the emission bands in the QDP spectra. Representative low (0.2 W/cm^2, black line) and high (25 W/cm^2, red line) excitation density PL spectra recorded at the same spatial position are depicted in Fig. 6(a). These data are taken from a series of intensity-dependent spectra recorded at different spatial positions on the sample in the intensity range between 0.2 and 250 W/cm^2. Several of the spectrally sharp resonances display linear excitation intensity dependence and reflect the emission from excitonic (X) states localized within these QDs. When normalizing these spectra to the X emission intensity, it is clearly evident that for each X line a connected XX line exists, which is redshifted by 1–3 meV and displays a nonlinear intensity dependence. This assignment is clearly supported by plotting the dependence of the peak intensity of all these lines on the excitation power. We have studied this excitation power dependence for several individual QD pairs and representative results are shown in Fig. 6(b). The exciton lines of both QDs A and B show the same, essentially linear power dependence at low powers. Possibly, saturation of the high-energy QD-B sets in first. Studying different QDs, we observe that sometimes the low-energy and sometimes the high-energy QD saturates first. The plots for the biexciton lines [dashed lines in Fig. 6(b)] indicate for both QDs a slope of 1.8, close to the ideally expected value of 2.

This power dependence supports the assignment of the X and XX lines to exciton and biexciton emissions from quantum-confined states localized within either quantum dot

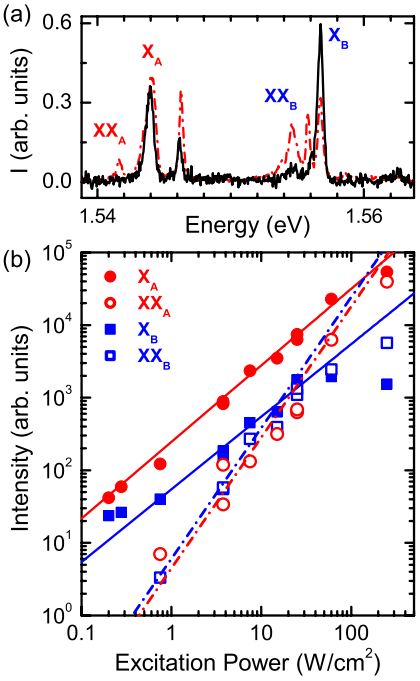

FIG. 6. (Color online) (a) Near-field PL spectra of an individual QD pair recorded at the same spatial position for two different excitation intensities of 0.2 W/cm^2 (red line) and 25 W/cm^2. Excitonic (X) and biexcitonic (XX) emission lines are distinguished by normalizing the two spectra to the intensity of the excitonic peak of QD-A. The emission line at 1.546 eV belongs to a different QDP. (b) Excitation power dependence of the intensity of the X and XX peaks of QD-A and QD-B of the individual QD pair studied in (a). The power dependence is plotted on a double-logarithmic scale. The solid lines are fits to a power dependence $I \propto P^{\alpha}$ with $\alpha = 1.05$ and 1.0 for X_A and X_B, respectively. The dashed lines indicate a power dependence $I \propto P^{\alpha}$ with $\alpha = 1.8$ for the biexciton peaks of the two QD.

A or B within the QDP. The power dependence also suggests that excitons are localized separately in the individual QDs of each pair. Apparently, there is no efficient tunnel coupling and also little incoherent exciton relaxation between the two dots of each pair. As stated before, the emission lines centered at 1.54 eV correspond to the geometrically somewhat larger QD-A. Excitonic and biexcitonic emissions account for most of the emission lines observed under high excitation intensity conditions as used for recording Fig. 3(a). In addition, we observe a few other spectrally sharp emission lines with lower emission intensity in the energy region of the X and XX lines. Even though the assignment of those lines is not yet conclusive, it is likely that this emission arises from charged excitonic states, as is well known from PL studies of Stranski-Krastanov QDs. At very high excitation intensities (>100 W/cm^2), we find additional emission lines at the energy of about 20 meV above the X emission. Our results indicate that this emission stems from excited excitonic states within these QDs. This indicates a sublevel splitting of about 20 meV within the individual QDs of each pair, consistent with the dot diameter of about 90 nm estimated from the AFM measurements. Emission from these excited states is likely to account for the resonance appearing at the energy

of 18 meV above the A band in the density-dependent macroscopic PL spectra [Fig. 2(b)].

As a result, the following schematic picture for the energetic structure of the investigated QDPs emerges. For the present sample, the two QDs within each pair are spatially separated by about 130 nm, and excitons are localized within either the left or right dot of each pair. The geometries of these two dots are slightly different so that the energies of the lowest excitonic states vary slightly: around 1.54 eV for the geometrically larger dot and 1.55–1.6 eV for the geometrically smaller dot. Preliminary evidence exists for a sublevel splitting of about 20 meV within each QD.

The near-field results also help in clarifying the assignment of the far-field spectra in Fig. 2. The near-field results show conclusively that, also at very low optical powers, emission from both the low- and high-energy dots is observed. The emission from the low-energy dot falls into the energy range around 1.54 eV, whereas that of the high-energy dot scatters more strongly and falls into the range from 1.56 to 1.58 eV. This makes it likely to assign the emission bands A and B in the far-field spectra at low powers to the inhomogeneously broadened emission spectra of the individual, high- and low-energy dots of each pair. The near-field data show essentially the same power dependence for the excitonic and biexcitonic emission peaks of both dots. Therefore, one can clearly not explain the power dependence of the far-field spectra by considering the ground state excitonic emission of both dots only. Obviously, saturation of the ground state emission and increasing emission from excited states at lower optical powers must be taken into account in order to explain the power dependence.

A statistical average of the near-field emission spectra in Fig. 3, recorded at an intermediate excitation intensity of about 75 W/cm^2, confirms this conclusion. In this analysis (Fig. 7), we identified the spatial center position of each emission peak in the near-field spectra and assigned it to either the low- or high-energy dot of each pair. This assignment procedure was performed for more than 200 emission peaks and resulted in the histograms shown in Fig. 7(a) for the low- and high-energy dots, respectively. When convoluted with a Lorentzian line shape function with a width of 4 meV, these histograms gave the ensemble-averaged spectra shown as a dashed red line (low-energy dot) and as a dashed-dotted blue line (high-energy dot) in Fig. 7(b), respectively. The summation of both spectra (solid black line) qualitatively resembles the far-field spectrum at such intermediate excitation intensities.

The average spectrum of the low-energy dot (dashed red line) is dominated by the strong ground state emission peak (the A band in the far-field spectrum) around 1.54 eV. Slight differences in the emission energies between ensemble-averaged near-field and far-field spectra are likely to arise from a different inhomogeneously broadened ensemble probed in both experiments and/or the different spectrometers used. In addition to the ground state emission, this spectrum shows a shoulder at higher energies, most likely arising from excited state emission.

The emission of the high-energy dot (dashed-dotted blue line) shows a complicated emission spectrum in the energy region of the B band, with contributions from excitons in both ground and excited states. Therefore, at intermediate excitation intensities, the band B in the far-field spectrum can no longer be assigned to ground state emission from the high-energy dot alone. Rather it reflects a complicated superposition of different emission bands, namely, exciton and biexciton ground state emissions of the high-energy dot and excited state emission from both dots.

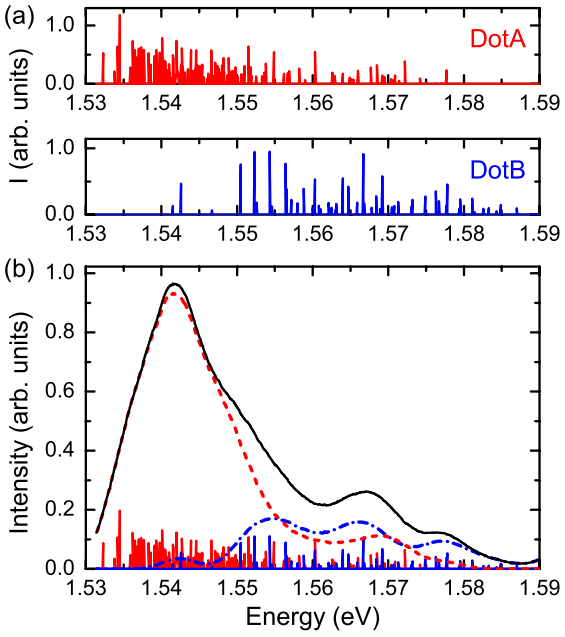

FIG. 7. (Color online) [(a), Top] Histogram of the spectral distribution of the near-field PL intensities of the emission peaks of the low-energy dot. For each emission peak in the near field in Fig. 3(a), the spatial center position is identified to either the low- or high-energy dot of the respective QD pair. For the sampled statistical ensemble of low-energy dot peaks, the emission intensity is then plotted as a function of the emission energy. [(a), Bottom] Histogram of the spectral distribution of the near-field PL intensities of the emission peaks of the high-energy dot. (b) Ensemble-averaged emission spectra of the low-energy (dashed red line) and high-energy (dashed-dotted blue) quantum dots. The spectra are extracted by convoluting the histograms in (a) with a Lorentzian line shape function with a width of 4 meV. The summation of both spectra is shown as a solid black line.

This supports the assignment of the intensity-dependent far-field spectra given already above. The intense band A reflects the ground state (excitonic and biexcitonic) emission of the low-energy dot. At low excitation densities, the emission of band B is governed by ground state emission from the high-energy dot. At higher energies, luminescence from excited exciton states of both dots adds to this emission band. With increasing excitation intensity, the ground state emission saturates, and excited state emission in the energy range of the B band dominates the spectrum.

V. SUMMARY AND CONCLUSIONS

In summary, the results reported in this paper give experimental evidence for a correlation between structural and optical properties of QDs grown by droplet epitaxy. By means

of a statistical analysis of low-temperature near-field PL spectra, we have demonstrated that the geometric alignment and interdot spacing of 130 nm found in AFM images of uncapped quantum dot pairs also govern the optical properties of these nanostructures. Quantitative information on the energetics of confined excitonic states within such pairs is obtained. For conceptual simplicity, these PL studies have been performed on QDPs with a rather large interdot separation, where the formation of coherently coupled molecular quantum dot states is suppressed and in which excitonic interactions between neighboring dots within each pair are weak. During the past months, several research groups have demonstrated that droplet epitaxy permits the growth of pairs and more complex arrays of QDs with much smaller dimensions and interdot distances in the range of a few tens of nanometers. The excellent optical properties of droplet epitaxy QDs demonstrated in our work make such pairs and arrays highly interesting for probing the intricate optical properties of molecular excitonic states and in particular the complex dynamics of dipolar interactions in quantum dot arrays with controlled geometries. Such studies are highly relevant for exploring the potential of these nanostructures for implementing scalable arrays of exciton and/or spin-based quantum bits and are now under study.

ACKNOWLEDGMENTS

The authors acknowledge the financial support of the Deutsche Forschungsgemeinschaft via the Sonderforschungsbereich 296 and National Science Foundation of US through Grant No. DMR-0520550. One of the authors (R.P.) also greatly acknowledges the financial support from Humboldt Graduate School.

*robert.pomraenke@uni-oldenburg.de

†On leave from Institute of Semiconductor Physics, National Academy of Sciences of Ukraine, prospect Nauki 41, 03028 Kiev, Ukraine.

[1] T. H. Stievater, X. Q. Li, D. G. Steel, D. Gammon, D. S. Katzer, D. Park, C. Piermarocchi, and L. J. Sham, Phys. Rev. Lett. **87**, 133603 (2001).

[2] A. Zrenner, E. Beham, S. Stufler, F. Findeis, M. Bichler, and G. Abstreiter, Nature (London) **418**, 612 (2002).

[3] X. Q. Li, Y. W. Wu, D. Steel, D. Gammon, T. H. Stievater, D. S. Katzer, D. Park, C. Piermarocchi, and L. J. Sham, Science **301**, 809 (2003).

[4] J. P. Reithmaier, G. Sek, A. Loffler, C. Hofmann, S. Kuhn, S. Reitzenstein, L. V. Keldysh, V. D. Kulakovskii, T. L. Reinecke, and A. Forchel, Nature (London) **432**, 197 (2004).

[5] T. Yoshie, A. Scherer, J. Hendrickson, G. Khitrova, H. M. Gibbs, G. Rupper, C. Ell, O. B. Shchekin, and D. G. Deppe, Nature (London) **432**, 200 (2004).

[6] A. Badolato, K. Hennessy, M. Atature, J. Dreiser, E. Hu, P. M. Petroff, and A. Imamoglu, Science **308**, 1158 (2005).

[7] T. Unold, K. Mueller, C. Lienau, T. Elsaesser, and A. D. Wieck, Phys. Rev. Lett. **94**, 137404 (2005).

[8] M. Kroutvar, Y. Ducommun, D. Heiss, M. Bichle, D. Schuh, G. Abstreiter, and J. J. Finley, Nature (London) **432**, 81 (2005).

[9] A. Greilich, D. R. Yakovlev, A. Shabaev, A. L. Efros, I. A. Yugova, R. Oulton, V. Stavarache, D. Reuter, A. Wieck, and M. Bayer, Science **313**, 341 (2006).

[10] F. H. L. Koppens, C. Buizert, K. J. Tielrooij, I. T. Vink, C. K. Nowack, T. Meunier, L. P. Kouwenhoven, and L. M. K. Vandersypen, Nature (London) **442**, 766 (2006).

[11] Q. Xie, A. Madhukar, P. Chen, and N. P. Kobayashi, Phys. Rev. Lett. **75**, 2542 (1995).

[12] M. Schmidbauer, S. Seydmohamadi, D. Grigoriev, Z. M. Wang, Y. I. Mazur, P. Schafer, M. Hanke, R. Kohler, and G. J. Salamo, Phys. Rev. Lett. **96**, 066108 (2006).

[13] T. Mano, R. Notzel, G. J. Hamhuis, T. J. Eijkemans, and J. H. Wolter, Appl. Phys. Lett. **81**, 1705 (2002).

[14] B. Krause, T. H. Metzger, A. Rastelli, R. Songmuang, S. Kiravittaya, and O. G. Schmidt, Phys. Rev. B **72**, 085339 (2005).

[15] S. C. Lee, L. R. Dawson, K. J. Malloy, and S. R. Brueck, Appl. Phys. Lett. **79**, 2630 (2001).

[16] T. Mano, T. Kuroda, S. Sanguinetti, T. Ochiai, T. Tateno, J. Kim, T. Noda, M. Kawabe, K. Sakoda, G. Kido, and N. Koguchi, Nano Lett. **5**, 425 (2005).

[17] Zh. M. Wang, K. Holmes, J. L. Shultz, and G. J. Salamo, Phys. Status Solidi A **202**, R85 (2005).

[18] B. L. Liang, Zh. M. Wang, J. H. Lee, K. Sablon, Yu. I. Mazur, and G. J. Salamo, Appl. Phys. Lett. **89**, 043113 (2006).

[19] Zh. M. Wang, K. Holmes, Yu. I. Mazur, K. A. Ramsey, and G. J. Salamo, Nanoscale Res. Lett. **1**, 57 (2006).

[20] J. H. Lee, Zh. M. Wang, N. W. Strom, Yu. I. Mazur, and G. J. Salamo, Appl. Phys. Lett. **89**, 202101 (2006).

[21] M. Yamagiwa, T. Mano, T. Kuroda, T. Tateno, K. Sakoda, G. Kido, N. Koguchi, and F. Minami, Appl. Phys. Lett. **89**, 113115 (2006).

[22] A. Richter, G. Behme, M. Süptitz, C. Lienau, T. Elsaesser, M. Ramsteiner, R. Nötzel, and K. H. Ploog, Phys. Rev. Lett. **79**, 2145 (1997).

[23] C. Lienau, Philos. Trans. R. Soc. London, Ser. A **362**, 861 (2004).

[24] K. Karrai and R. D. Grober, Appl. Phys. Lett. **66**, 1842 (1995).

[25] F. Intonti, V. Emiliani, C. Lienau, T. Elsaesser, R. Nötzel, and K. H. Ploog, Phys. Rev. B **63**, 075313 (2001).

[26] M. Hanke, M. Schmidbauer, D. Grigoriev, P. Schäfer, R. Köhler, T. H. Metzger, Z. Wang, Y. Mazur, and G. J. Salamo, Appl. Phys. Lett. **89**, 053116 (2006).

[27] *Properties of Gallium Arsenide*, EMIS Data Reviews Series No. 2 (The Institute of Electrical Engineers, London, 1990).

[28] M. Bayer, T. Gutbrod, A. Forchel, V. D. Kulakovskii, A. Gorbunov, M. Michel, R. Steffen, and K. H. Wang, Phys. Rev. B **58**, 4740 (1998).

[29] P. Lambelet, A. Sayah, M. Pfeffer, C. Philipona, and F. Marquis-Weible, Appl. Opt. **37**, 7289 (1998).